RSC Advances

ROYAL SOCIETY OF CHEMISTRY

www.rsc.org/advances

Table of Contents Entry

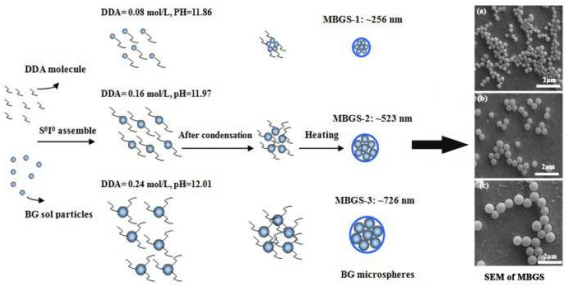

Highlight:

Monodispersed mesoporous bioactive glass sub-micron spheres with with controllable size and good biocompatibility were fabricated by improved sol-gel method.

Size control and biological properties of monodispersed mesoporous bioactive glass sub-micron spheres

Qing Hu[1,2,3], Yuli Li[1,2,3], Guohou Miao[1,2,3], Naru Zhao[1,2,3], Xiaofeng Chen*[1,2,3]

[1] School of Materials Science and Engineering, South China University of Technology, Guangzhou 510641, P.R China.

[2] National Engineering Research Center for Tissue Restoration and Reconstruction, Guangzhou 510006, China.

[3] Guangdong Province Key Laboratory of Biomedical Engineering, South China University of Technology, Guangzhou 510006, China.

* Corresponding author. Tel.: +86 20 2223 6283; fax: +86 20 2223 6088

E-mail addresses: chenxf@scut.edu.cn

Abstract

We report a facile method for fabricating monodispersed mesoporous bioactive glass sub-micron spheres (MBGS) using dodecylamine (DDA) as a catalyst and template agent in sol-gel process through self-assembly between neutral organic surfactant and neutral inorganic precursor (S^0I^0), and investigate the effect of sub-micron particle size on physicochemical properties, apatite-forming ability, and biocompatibility of MBGS. Results showed that all samples exhibited regularly spherical morphology and favorable mono-dispersibility. The average particle diameters of the MBGS (200 nm~ 800 nm) were controlled by adjusting the concentration of DDA. All samples induced the formation of rod-like apatite precipitates which were more close to natural nanoscale apatite crystal, showing the high apatite-forming ability. Furthermore, MBGS surfaces also supported attachment and promoted proliferation, alkaline phosphatase (ALP) activity of MG-63 cells, showing the good biocompatibility of MBGS. MBGS-1 possessing with a smallest particle size could significantly enhanced MG-63 proliferation and differentiation because of their smaller particle size, higher specific surface area. This study may motivate the development and applications of submicron-biomaterials in bone repair.

Key words: bioactive glass; monodispersed; sub-micron spheres; controllable size; apatite formation; biocompatibility.

1. Introduction

Bioactive glasses (BGs) have been widely used for bone tissue regeneration because of their good osteoconductive, osteoproductive and osteoinductive properties as well as causing minimal inflammatory response of the host after implantation.[1-5] In the past few years, scientists have been focused on developing various BGs materials.[6-8] Many studies suggested that the bone-bonding ability

of BGs can be due to the formation of a hydroxycarbonate apatite (HCA) layer on the BGs surface when they were contacting with the simulated body fluid (SBF).[9] Current commercially available BGs particles have the composition known as 45S5 Bioglass® (46.1 mol% SiO_2, 26.9 mol% CaO, 24.4 mol% Na_2O and 2.5 mol% P_2O_5) obtained by conventional melting method, which is used in a wide range of dental and orthopedic applications.[10-12] The particles are in the micrometer size-range and irregular in size and shape as well as exhibit a low-porosity texture with surface area in the range 0.15~2.7 m^2/g.[13, 14] On the other hand, compared with melting process, the sol-gel technology makes it possible to prepare BGs with unique micro/nano-scale structure and large surface area, which is very beneficial for their wider application.[4, 14-16]

Sol-gel processing, as a very versatile technique for producing inorganic particles with different morphologies and sizes by controlling the hydrolysis and condensation of organic precursors, has been introduced to biomaterials.[17, 18] The sol-gel derived BGs are considered to be a type of third-generation biomaterials because of their good bioactive, resorbable and osteoproductive properties.[1] It has been shown that sol-gel derived BGs have improved bioactivity and can enhance cell proliferation and differentiation, which is attributed to their unique surface textures.[19, 20] L.Meseguer-Olmo et al. found that the sol-gel derived BGs ceramic was bioactive, biocompatible and capable of promoting the mesenchymal stem cells differentiating into osteoblasts.[21] Jones et al. showed that the sol-gel derived BGs scaffolds supported the growth of primary human osteoblasts and induced their differentiation without adding supplementary factors.[22] However, the problems for sol-gel BGs are still unsolved, such as the severe agglomeration and irregular shape of BGs particles. Previous studies have shown that regular spherical BGs possess better physical-co-chemical and biological properties compared to the irregular BGs.[20] Moreover, spherical particles are the most suitable injectable materials because of their

good flow properties.[23-25]

Particle size can affect the efficiency and pathway of cellular uptake by influencing the adhesion of the particles and their interaction with cell.[26-28] Sub-micron BGs particles are an attractive alternative to BGs microparticles for hard tissue regeneration. Due to their specifical properties such as small size and high specific surface area, they are ideal materials for injecting into the bone defects or using as biopolymer reinforcement.[29, 30] In recent years, including our groups, several papers have reported the preparation methods and properties of spherical BGs particles.[7, 23, 24] However, the preparation of mono-dispersed spherical BGs particles with controllable size less than 1μm is very inconvenient. Although there has been increasing interest in fabricating sub-micron BGs spheres and corresponding composites, the sub-micron size effect was not clear in physicochemical and biological terms.[30, 31] Physicochemical properties and biocompatibility of BGs are related to their physical properties such as particle size, porosity, surface area, and morphology.[31] Before being used in any field, the physicochemical and biological properties of BGs should be evaluated carefully.

Therefore, in this study, we show a facile sol-gel method to fabricate monodispersed mesoporous bioactive glass sub-micron spheres (MBGS) with controllable particle size using dodecylamine (DDA) as a catalyst and template agent. DDA is a kind of organic weak base with amphipathy, which is usually used as template to synthetize mesoporous materials.[32-34] We focused on investigating the effect of sub-micron particle size on physicochemical properties, apatite-forming bioactivity, and biocompatibility.

2. Materials and methods

2.1 Synthesis of MBGS

MBGS with a molar composition of 80% SiO_2, 16% CaO and 4% P_2O_5 were synthesized by

improved sol-gel method using dodecylamine (DDA, Aladdin) as a catalyst and template agent. The typical procedure for fabricating MBGS was performed according to a previous publication.[35] Briefly, a given amount of DDA was dissolved in 25 ml deionized water (DW) and 80 ml absolute ethanol (ETOH, Guanghua Chemical). When DDA was dissolved completely, 16 ml tetraethyl orthosilicate (TEOS, Guanghua Chemical), 1.22 ml triethylphosphate (TEP, Aladdin) and 3.39 g calcium nitrate tetrahydrate (CN, Guanghua Chemical) were added to the above solutions in order for 30 min interval with magnetically stirring at 40 °C. The resulted solution was vigorously stirred together for another 3 h, the clear solutions gradually turned into opaque due to the formation of a white precipitate. The white precipitate was collected by filtration and in turn rinsed with absolute ethanol and deionized water for three times, dried under vacuum at room temperature for 24 h. The MBGS was obtained after removing templates and organic components by sintering in air at 650 °C for 3 h (2 °C /min). In this study, the concentration of DDA determined the MBGS size. Therefore, DDA concentrations of 0.08 mol/L, 0.16 mol/L and 0.24 mol/L were used and the corresponding MBGS were denoted MBGS-1, MBGS-2 and MBGS-3, respectively. Besides, in order to interpret the formation mechanism of the MBGS more clearly, a few samples without the DDA and with higher concentration of DDA (0.4 mol/L) were also synthesized.

2.2 Morphology, structure, composition and size distribution measurements

The morphology and monodispersity of the prepared MBGS were determined using field emission scanning electron microscope (FE-SEM, Nova NanoSEM430, FEI, USA). Before observation, the particles were coated with gold for 180 seconds under a gas pressure of 50 mTorr. The specific surface area and pore volume were evaluated using multipoint Brumauer-Emmett-Teller (BET) N_2 absorption technique at 77.3 K.[36] The pore size was calculated by the Barrett-Joyner-Halenda (BJH) method using

desorption isotherm branch. The elemental compositions were recorded by energy dispersive spectroscopy (EDS). The particle size distributions of samples were tested by Zetasizer Nano-ZS.

2.3 Assessment of apatite-forming ability

The assessment of the apatite-forming ability of the obtained MBGS was tested by immersing samples in SBF described by Kokubo et al.[37] (Na^+ 142.0, K^+ 5.0, Mg^{2+} 1.5, Ca^{2+} 2.5, Cl^- 147.8, HCO^{3-} 4.2, HPO_4^{2-} 1.0, and SO_4^{2-} 0.5 mmol L^{-1}) at a concentration of 1mg/ml at 37 °C to monitor the formation of HCA on the surface of the samples with time. All the samples were soaked in SBF for 3 days without refreshing solution. Once removed from the incubation, the solids were separated by centrifugation, washed three times with acetone and deionized water, then dried at ambient temperature and characterized using transmission electron microscopy (TEM, JEM-2100HR, Japan, 100 kV), Fourier transform infrared spectroscopy (FT-IR, Nexus, Nicolet Co., USA) and powder X-ray diffraction (XRD, X'pert PRO, Panalytical, the Netherlands) with Cu K_a (1.548 Å).

2.4 Culture of MG-63 human osteoblast-like cells

Human osteoblast-like cells MG-63 (American Type Culture Collection), originally isolated from a human osteosarcoma,[38] were used for the experiments. MG-63 cells are relatively immature osteoblasts that have been well characterized and widely used for testing biomaterials,[39-42] and show numerous osteoblastic traits.[43, 44] MG-63 cells were grown in tissue culture flasks in completed Dulbecco's Modified Eagles Medium (DMEM) containing 10% (v/v) fetal bovine serum (FBS). The cells were cultured at 37 °C in a 5% CO_2 atmosphere and 95% of relative humidity to allow the MG-63 to adhere. The culture media was changed every 2-3 days and the non-adherent cells were washed away by phosphate buffer solution (PBS). When the MG-63 cells were cultured until 80% confluence, the confluent cells were detached by trypsin and used for the seeding, attachment, proliferation and

differentiation assays.

2.5 MG-63 seeding and culture on MBGS

Preparation of the interfaces of MBGS for cell culture: To observing the MG-63 attachment behavior on the interfaces of MBGS particles, the MBGS particles were coated on the surface of glass slides (Dingjie Biotech., China).[20] Before coating, the slides were cut into squares (1 cm^2) using a diamond glass cutter, ultrasonically cleaned for 5 min in absolute ethanol and deionized water respectively and then dried at 120 °C for 2 h. MBGS particles were deposited by a spin coating process (WS-400B-6NPP-LITE, Laurell Tech.Co., USA). Briefly, 200 μl suspensions of MBGS particles (dissolved in absolute ethanol at a concentration of 1mg/ml) were added onto the surface with the samples spun at 1000 rpm for 10 seconds, which was repeated 5 times for each sample. Finally, the prepared samples were dried at 60 °C for 2 h and sterilized by autoclave.

Cell culture on MBGS particles: Before seeding, the glass slides containing MBGS particles were incubated in DMEM at 37 °C for 24 h. Cells were digested and seeded on MBGS at a density of 2×10^4 cells cm^{-2} in 24 well plates. Then the samples were incubated at 37 °C with 5% CO_2 for 2 h to allow the cells to attach. The wells were then flooded with culture media and cultured for a different number of days.

2.6 Attachment and proliferation evaluation of MG-63

The attachment morphology of MG-63 on the surface of MBGS was qualitatively assessed by environmental scanning electronic microscopy (ESEM, Quanta200, FEI, Netherlands) after culturing for 4 h. For the ESEM observations, MG-63 cells were fixed by 2.5% glutaraldehyde for 30 min and dehydrated using gradient ethanol concentrations (5%, 70%, 80%, 90%, 95% and 100% v/v in water). After drying at a room temperature, the samples were coated with gold for 180 seconds under a gas

pressure of 50 mTorr and observed by ESEM. To further understand the adherence and growth behavior of MG-63, the fluorescence microscopy (FM, 40FLAxioskop, Zeiss, Germany) was used after culturing for 3 days. For the FM assessment, MG-63 cells were stained using a live cells labeling kit (Cell Explorer, AAT Bioquest). The staining process was according to the kit instructions. In brief, at the time point, the culture medium was replaced by the staining solution, incubated at 37 °C for 1 h, followed by washing with PBS and then observed by FM.

The cells proliferation was quantitatively determined by a colorimetric assay based on the conversion of 2-(2-methoxy-4nitrophenyl)-3-(4-nitrophenyl)-5-(2, 4-disulfophenyl)-2H-tetraxolium, monosodium salt (WST-8) into the highly water soluble formazan, enabling the assessment of the number of cells,[45] which was evaluated using a cell counting kit (CCK-8) in accordance with the manufacturer's instructions. Briefly, cells were seeded at a concentration of 3×10^3 cells cm^{-1} onto a 96-well plate and cultured for 1 d at 37 °C in a humidified atmosphere of 95% air and 5% CO_2. Pure tissue culture plastic templates (TCP) were used as a control. After cultured for 1 d, the culture medium was refreshed by 200 μl suspensions of MBGS particles (dissolved in DMEM at a concentration of 100 μg/ml), followed by incubation for 1, 3, 5 and 7 days. At the time point, samples were washed with PBS and 200 μl CCK-8 mixture solutions (0.5 mg/ml) were added to each well, followed by incubation for 2 h. The absorbance was measured at a wavelength of 450 nm using a micro-plate reader (Thermo 3001, Thermo Co., USA). Six specimens for each culture time point were tested and each test was performed in triplicate.

2.7 ALP activity assay

The osteogenic differentiation of MG-63 cultured on the MBGS particles and TCP was assessed by measuring the ALP activity using p-nitrophenyl phosphate substrate (pN) (ALP kit, Thermochem).

At 5 and 10 days, the culture medium was removed and the cell layers were rinsed gently 3 times using cold PBS. The cells were lysed and lysate was assayed with the hydrolysis of pN in the presence of ALP enzyme. This evaluation was performed in accordance to the manufacturer's instructions (Sigma, USA) and the absorbance was measured at a wavelength of 405 nm using a microplate reader. A sample cultured under the same conditions without cells was used as a blank to correct the absorbance values. After normalizing to the total protein content, the ALP activity was calculated from a standard curve. The total protein content was examined using a Pierce BCA protein assay kit (Thermo Scientific, USA) and the results expressed as μmol of pN produced per milligram of protein. Three individual experiments were carried out and each sample was conducted in quadruplicate.

2.8 Statistical analysis

All date are expressed as mean ± standard deviation (SD) and were analyzed using a Student's t-test. A p-value < 0.05 was considered statistically significant.

3. Results

3.1 Morphology, size distribution, structure and composition of MBGS

In our study, monodispersed spherical bioactive glass particles with controllable size less than 1 μm were successfully synthesized by improved sol-gel method using DDA as a hydrolysis catalyst. As shown in Fig. 1 a, b, c, all samples exhibit regularly spherical morphology and favorable mono-dispersibility, which perfectly solves the agglomeration problem of the conventional sol-gel BGs. By adjusting the concentration of DDA to 0.08 mol/L, 0.16 mol/L and 0.24 mol/L, the average particle diameters of MBGS were 256±25 nm (MBGS-1), 523±32 nm (MBGS-2) and 716±54 nm (MBGS-3) respectively, as shown in Fig. 2. Furthermore, as we can see from the amplifying images (Fig.1 d, e, f), all the MBGS particles show relatively rough surface. It was supposed that a bioactive glass sphere was

composed by the accumualtion of numerous nano-particles, which result in nanoscale surface morphology. However, when adding no DDA, TEOS couldn't be hydrolyzed effectively, the reaction solutions kept clear due to producing no white precipitate, which means that MBGS couldn't be obtained without adding the DDA. The photos for the state of the reaction solutions without the DDA and with the DDA were shown in Fig. 3 a, b. When adding excessive concentration of DDA (0.4mol/L), MBGS particles became irregular, as shown in Fig. 3 c.

Fig.4 shows N_2 absorption-desorption isotherm plots and pore size distributions of MBGS, and the BET specific surface areas, the total pore volumes and mean pore sizes were listed in Table 1. The results suggested that the average pore diameters for MBGS were characteristic of mesoporous materials. Furthermore, the specific surface areas of MBGS were much higher than the conventional melt- derived BGs and significantly increased with decreasing MBGS particles size. Fig. 5 shows the crystalline phase structure and chemical composition of the MGBS. All the MBGS prepared in this study displayed the representative amorphous nature with a broad peak $2\theta=23^{\circ}$. The presence of silicon (Si), calcium (Ca), phosphorus (P) and oxygen (O) was clear by EDS analysis. The analysis of the relative intensity of these peaks indicated the molar ratio of SiO_2: CaO: P_2O_5 is ~ 84: 12: 4.

3.2 *In vitro* apatite-forming ability of MBGS

The *in vitro* apatite-forming ability is the important property of bioactive glass materials, which influences directly the bone-forming activity *in vivo*.[37] Here, the apatite-forming ability of MBGS with different sizes was tested by immersing samples in SBF for 3 days. The representative morphologies of the samples after soaking in SBF were shown in Fig. 6. After soaking in SBF for 3 days, the surfaces of all the samples were covered by rod-like apatite precipitates, which aggregated together and intertwined with each other. Additionally, the rod-like apatite precipitates

were more close to natural nanoscale apatite crystal, the diameters and lengths of the precipitates were 20~30 nm and 100~200 nm, respectively. The TEM image of natural nanoscale apatite crystal obtained by H. D. Wagner [46] was shown in Fig. 7. The precipitates were confirmed to be hydroxyapatite (HA) crystal according to the FT-IR and XRD results.

The crystalline structure of the apatite layer precipitated on the surface of the MBGS after immersing in SBF was identified by XRD analysis, as shown in Fig. 8a. By comparing with the XRD patterns before soaking (Fig. 5a), new peaks were observed at 2θ= 26º (002), 32º (211), 39º (310), 46º (222), 49º (213) and 53º (004) corresponding to the crystallinity for HA (JCPDS 09-0432). It meant that all the samples could induce the formation of HA with poor crystallinity after soaking in SBF for 3 days.

The formation of the crystalline HA layer after immersing in SBF was also demonstrated by FT-IR analysis, as shown in Fig. 8b. Before soaking (data not shown), the spectrum of all the MBGS exhibited characteristic absorption bands corresponding to Si-O-Si bonding at 1060 (stretch vibration), 798 (bending vibration), and 480 cm^{-1} (bending vibration).[35] After 3 d of soaking in SBF, a double band at 562 and 603 cm^{-1} corresponding to the P-O bending vibrations of phosphate groups in a crystalline environment can be observed. The presence of absorption bands of the phosphate groups at 968, 603, and 562 cm^{-1} demonstrates the deposition of HA on the surface of MBGS. Based on the analysis of TEM, XRD and FT-IR, it is evident that all the samples possess good apatite-forming ability.

3.3 Biocompatibility of MBGS

It has been well understood that the attachment of cells is the fundamental process of cell proliferation, differentiation and its function are governed by the interaction of cells with their substrate.[47] In order to reveal the cells attachment to the surfaces of the MBGS, MG-63 cells cultured

on the surfaces of MBGS for 4 h were examined by ESEM, as shown in Fig. 9. It was evident that MG-63 cells could attach and spread well on MBGS-1 (Fig. 9a), MBGS-2 (Fig. 9b) and MBGS-3 (Fig. 9c). The FM images further indicate that MG-63 cells spread well and exhibit good viability on all samples after cultured for 3 d, as shown in Fig. 10. Accordingly, ESEM and FM images of cells qualitatively show that all the MBGS surfaces have good cell attachment and spread properties.

CCK-8 tests were used to quantitatively determine the cell proliferation on the surfaces of MBGS after culturing for 1, 3, 5 and 7 days, as shown in Fig. 11. It was obvious that the cells presented stable proliferation ability on all MBGS with the culture time increased. MBGS-1 showed slightly higher cell proliferation than MBGS-2, MBGS-3 and control at a culture time of 1 day. Up to 7 days, MG-63 cells displayed significantly higher proliferation ability on MBGS-1 and MBGS-2, as compare to control. Furthermore, the cell proliferation ability enhanced as decreasing MBGS particles size. The results suggest that MBGS promote MG-63 cell proliferation and decreasing the particle size could improve the cell proliferation ability.

It is well known that ALP activity is an obvious osteogenic mark indicating the cell differentiation ability. To quantitatively investigate the effect of the MBGS size on the osteogenic differentiation of MG-63, the ALP activity was performed on day 5 and 10 after culturing on the surfaces of MBGS. As shown in Fig. 12, the ALP activity expression of all the MBGS increased with the culture time increased. At 5 days, the ALP activity expression of all the MBGS were comparable to the baseline ALP for MG-63 on tissue culture plate as a control, the data didn't have significant differences. Up to 10 days, the ALP activity expression of all the MBGS presented greater than control, Furthermore, the ALP activity also increased as decreasing MBGS particles size.

4. Discussions

Sub-micron spherical BGs have been paid great attention in the applications of bone tissue regeneration because of their specialties such as small size, high specific surface area and mimicking the extracellular matrix.[48] However, it is not easy to prepare mono-dispersed spherical BGs particles with controllable size less than 1μm, so the effect of sub-micron particle size on physicochemical properties, apatite-forming bioactivity, and biocompatibility was not clear.

In this paper, we present a facile sol-gel method to fabricate MBGS with controllable particle size (200 nm ~ 800 nm) using DDA as a catalyst and template agent. Fig.10 shows the schematic illustration of the formation processes of MBGS. MBGS were synthetized through self-assembly between neutral organic surfactant and neutral inorganic precursor (S^0I^0).[32, 49-51] DDA was used as the structure directing surfactant (S^0) and BG sols as the inorganic precursor (I^0). The S^0I^0 assembly relies on hydrogen bonding between S^0 and I^0 at the micelle interface, and will proceed during the formation of silica oligomer generated by the hydrolysis of TEOS. Without adding the DDA, TEOS couldn't be hydrolyzed effectively which resulted that the reaction couldn't be proceed. Furthermore, DDA is a kind of organic weak base, in the ethanol/water solvent, the condensation reaction is controlled by using base catalysts which prevents the particles fusing together and further favors the formation of regularly spherical particles.[29, 52, 53] By adjusting the concentration of DDA, the average particle diameters of MBGS were controlled. This may be ascribed to the fact that the growth of the MBGS particles is significantly influenced due to the charged DDA concentration and its assembling with BGs sol. The higher DDA concentration could form the larger surfactant template and the bigger DDA-BG assembly, which could explain that high DDA produced the big MBGS particles. However, excessive concentration of DDA produce higher pH values where faster condensation provides wide size distribution of nuclei that grow for rapid aggregation of particles, leading to irregular shape as well as

formation of large aggregates larger BGs particles.[54] Finally, After calcinations, DDA was removed, leaving behind the mesoporous structure.[35] All the MBGS displayed relatively higher specific surface areas, as compared to conventional melt-derived BGs. The significant improvement in specific surface area for MBGS was due to the small size effects and coarse surface. XRD and EDS analysis indicated that the as-prepared MBGS kept the amorphous structure and consistent chemical composition. The results above demonstrated that monodispersed mesoporous bioactive glass sub-micron spheres with controlled size and uniform structure were fabricated successfully.

It has been commonly accepted that the ability of apatite formation in a physiological environment is the evidence of bioactivity for BGs. Here, the high specific surface area of MBGS might provide more reactive sites on the surface of the particles, and the spherical morphology could facilitate the exchange of ions and stimulate the apatite deposition from SBF.[55] Therefore, the high apatite-forming ability could be expected for the MBGS particles produced in this work. The results of apatite-forming ability test showed that all samples induce the formation of rod-like apatite precipitates which were more close to natural nanoscale apatite crystal in 3 days, showing the high apatite-forming ability.

Some publications reported that decreasing size or increasing specific surface area of BGs particles may not only improve apatite-forming ability, but also stimulate the cell compatibility.[15, 18, 56] However, few studies focus on investigating the cellular biocompatibility of sub-micron spherical BGs particles with controlled particles sizes. Therefore, in this study, we studied the effects of MBGS with different sizes on the attachment, proliferation and ALP differentiation of MG-63 cells. Our results indicated that cells adhere, spread and exhibit good viability well on all samples. Additionally, the CCK-8 quantitative results suggested that all the MBGS could promote MG-63 cell proliferation and decreasing the particle size could improve the cell proliferation ability. Differentiation of cells is one of

the key processes for bone regeneration. ALP is a cell surface glycoprotein, which is the most widely recognized marker of osteoblastic differentiation.[57] The MG-63 cultured on all the MBGS presented the higher ALP activity expression as compared with control at 10 days. Furthermore, the ALP activity increased as decreasing MBGS particles size.

Apparently, the results presented in this study demonstrated that all the MBGS could promote proliferation and ALP differentiation of MG-63 cells and MBGS-1 with a smallest particle size could significantly increase the proliferation and differentiation of cells, as compared to MBGS-2 and MBGS-3. It is well known that the physical properties such as particle size and surface area, chemical properties such as release of silicon ions from BGs may be the important factors influencing cellular biocompatibility of biomaterials.[58, 59] A higher specific surface area might provide more adsorptive sites on the surface of the particles, and subsequently enhance protein and growth factor adsorption, which is help for subsequent cell adherence and proliferation.[30, 31, 60] The effect of ionic products such as Si from BGs dissolution on cell proliferation and differentiation has been extensively investigated.[61, 62] Valerio et al. found osteoblast proliferation and osteoblast activity was increased mainly by the Si from BGs dissolution.[61] In our study, MBGS-1 possessing with a smaller particles size and higher specific surface area would enhance the contact surface area between MBGS-1 and medium, which might increase ionic products concentrations compared with MBGS-2 and MBGS-3. [30] It could also explain that MBGS-1 presented higher cells proliferation and differentiation ability. Further study will be necessary to understand the mechanism of the size effects of MBGS on cells proliferation and differentiation.

5. Conclusion

Our results demonstrated that MBGS with controllable size less than 1 μm and uniform structure were successfully fabricated by improved sol-gel method using DDA as a hydrolysis catalyst and

template agent. This study effectively solved the problems of the severe agglomeration, irregular shape, uncontrollable size and low specific surface area of the conventional BGs particles. All samples induced the formation of rod-like apatite precipitates which were more close to natural nanoscale apatite crystal, showing the high apatite-forming ability. MBGS surfaces also support attachment and promote proliferation and ALP differentiation of MG-63 cells, showing the good biocompatibility of MBGS. MBGS-1 possessing with a smallest particle size could significantly enhanced MG-63 proliferation and differentiation because of their smaller particle size, higher specific surface area. Further study to understand the mechanism of the size effects of MBGS on MG-63 proliferation and differentiation is in progress. These results suggest that MBGS with controllable size can be used as a more promising biomaterial for bone repair.

Acknowledgements

This work was supported by the National 973 project of China (2011CB606204), National Natural Science Foundation of China (Grant No. 51172073, 51202069, 51372005), Research Fund for the Doctoral Program of Higher Education of China (20110172110002) and the Fundamental Research Funds for the Central University (2012ZP0001).

References

1. L. L. Hench and J. M. Polak, *Science*, 2002, **295**, 1014.
2. L. L. Hench, *J Am Ceram Soc*, 1991, **74**, 1487-1510.
3. L. L. Hench, *Journal of Materials Science: Materials in Medicine*, 2006, **17**, 967-978.
4. H. Larry L, *Journal of the European Ceramic Society*, 2009, **29**, 1257-1265.
5. I. D. Xynos, A. J. Edgar, L. D. K. Buttery, L. L. Hench and J. M. Polak, *Journal of Biomedical Materials Research*, 2001, **55**, 151-157.
6. B. Lei, X. F. Chen, Y. J. Wang, N. R. Zhao, G. H. Miao, Z. M. Li and C. Lin, *Materials Letters*, 2010, **64**, 2293-2295.
7. B. Lei, X. Chen, Y. Wang and N. Zhao, *Materials Letters*, 2009, **63**, 1719-1721.
8. W. Chengtie, F. Wei, Z. Yufang, M. Gelinsky, C. Jiang, G. Cuniberti, V. Albrecht, T. Friis and X. Yin, *Acta Biomaterialia*, 2011, **7**.
9. L. L. Hench, R. J. Splinter, W. Allen and T. Greenlee, *Journal of Biomedical Materials*

Research, 1971, **5**, 117-141.
10. I. Xynos, M. Hukkanen, J. Batten, L. Buttery, L. Hench and J. Polak, *Calcified tissue international*, 2000, **67**, 321-329.
11. L. Hench, *Bioceramics*, 1994, **7**, 3-14.
12. M. Vollenweider, T. J. Brunner, S. Knecht, R. N. Grass, M. Zehnder, T. Imfeld and W. J. Stark, *Acta Biomaterialia*, 2007, **3**, 936-943.
13. P. Sepulveda, J. R. Jones and L. L. Hench, *Journal of Biomedical Materials Research*, 2001, **58**, 734-740.
14. I. A. Silver, J. Deas and M. Ereciska, *Biomaterials*, 2001, **22**, 175-185.
15. B. Lei, X. F. Chen, Y. J. Wang, N. Zhao, C. Du and L. M. Zhang, *Journal of Non-Crystalline Solids*, 2009, **355**, 2583-2587.
16. I. Cacciotti, M. Lombardi, A. Bianco, A. Ravaglioli and L. Montanaro, *Journal of Materials Science: Materials in Medicine*, 2012, **23**, 1849-1866.
17. D. Arcos and M. Vallet-Regi, *Acta Biomaterialia*, 2010, **6**, 2874-2888.
18. L. Bo and et al., *Biomed Mater*, 2010, **5**, 054103.
19. R. C. Bielby, R. S. Pryce, L. L. Hench and J. M. Polak, *Tissue Engineering*, 2005, **11**, 479-488.
20. B. Lei, X. Chen, X. Han and Z. Li, *J. Mater. Chem.*, 2011, **21**, 12725-12734.
21. L. Meseguer-Olmo, A. Bernabeu-Esclapez, E. Ros-Martinez, S. Sanchez-Salcedo, S. Padilla, A. Martin, M. Vallet-Regí, M. Clavel-Sainz, F. Lopez-Prats and C. Meseguer-Ortiz, *Acta Biomaterialia*, 2008, **4**, 1104-1113.
22. J. R. Jones, O. Tsigkou, E. E. Coates, M. M. Stevens, J. M. Polak and L. L. Hench, *Biomaterials*, 2007, **28**, 1653-1663.
23. B. Lei, X. F. Chen and Y. H. Koh, *J Sol-Gel Sci Techn*, 2011, **58**, 656-663.
24. B. Lei, K.-H. Shin, D.-Y. Noh, Y.-H. Koh, W.-Y. Choi and H.-E. Kim, *Journal of Biomedical Materials Research Part B: Applied Biomaterials*, 2012, **100B**, 967-975.
25. B. Lei, K.-H. Shin, Y.-W. Moon, D.-Y. Noh, Y.-H. Koh, Y. Jin and H.-E. Kim, *J Am Ceram Soc*, 2012, **95**, 30-33.
26. K. D. Lee, S. Nir and D. Papahadjopoulos, *Biochemistry*, 1993, **32**, 889-899.
27. H. Vallhov, S. Gabrielsson, M. Strømme, A. Scheynius and A. E. Garcia-Bennett, *Nano Lett*, 2007, **7**, 3576-3582.
28. F. Lu, S. H. Wu, Y. Hung and C. Y. Mou, *Small*, 2009, **5**, 1408-1413.
29. S. Labbaf, O. Tsigkou, K. H. Müller, M. M. Stevens, A. E. Porter and J. R. Jones, *Biomaterials*, 2011, **32**, 1010-1018.
30. B. Lei, X. Chen, X. Han and J. Zhou, *J Mater Chem*, 2012, **22**, 16906-16913.
31. Z. Hong, G. M. Luz, P. J. Hampel, M. Jin, A. Liu, X. Chen and J. F. Mano, *J Biomed Mater Res A*, 2010, **95**, 747-754.
32. P. T. Tanev and T. J. Pinnavaia, *Science*, 1995, **267**, 865-867.
33. J. Yu, L. Zhao and B. Cheng, *Journal of Solid State Chemistry*, 2006, **179**, 226-232.
34. X. Shi, Y. Wang, K. Wei, L. Ren and C. Lai, *Journal of Materials Science: Materials in Medicine*, 2008, **19**, 2933-2940.
35. Q. Hu, X. Chen, N. Zhao and Y. Li, *Materials Letters*, 2013, **106**, 452-455.
36. E. P. Barrett, L. G. Joyner and P. P. Halenda, *J Am Chem Soc*, 1951, **73**, 373-380.
37. T. Kokubo and H. Takadama, *Biomaterials*, 2006, **27**, 2907-2915.

38. D. J. Giard, S. A. Aaronson, G. J. Todaro, P. Arnstein, J. H. Kersey, H. Dosik and W. P. Parks, *Journal of the National Cancer Institute*, 1973, **51**, 1417-1423.
39. N. J. Hallab, C. Vermes, C. Messina, K. A. Roebuck, T. T. Glant and J. J. Jacobs, *Journal of Biomedical Materials Research*, 2002, **60**, 420-433.
40. F. Di Palma, M. Douet, C. Boachon, A. Guignandon, S. Peyroche, B. Forest, C. Alexandre, A. Chamson and A. Rattner, *Biomaterials*, 2003, **24**, 3139-3151.
41. F. Carinci, F. Pezzetti, S. Volinia, F. Francioso, D. Arcelli, J. Marchesini, E. Caramelli and A. Piattelli, *Clinical oral implants research*, 2004, **15**, 180-186.
42. P. Ramires, A. Romito, F. Cosentino and E. Milella, *Biomaterials*, 2001, **22**, 1467-1474.
43. J. Clover and M. Gowen, *Bone*, 1994, **15**, 585-591.
44. J. Martin, Z. Schwartz, T. Hummert, D. Schraub, J. Simpson, J. Lankford, D. Dean, D. Cochran and B. Boyan, *Journal of Biomedical Materials Research*, 1995, **29**, 389-401.
45. M. Ishiyama, Y. Miyazono, K. Sasamoto, Y. Ohkura and K. Ueno, *Talanta*, 1997, **44**, 1299-1305.
46. S. Weiner and H. D. Wagner, *Annual Review of Materials Science*, 1998, **28**, 271-298.
47. Y. Zhu, F. Shang, B. Li, Y. Dong, Y. Liu, M. R. Lohe, N. Hanagata and S. Kaskel, *Journal of Materials Chemistry B*, 2013, **1**, 1279-1288.
48. K. Kim and J. P. Fisher, *Journal of drug targeting*, 2007, **15**, 241-252.
49. R. Ryoo, I. S. Park, S. Jun, C. W. Lee, M. Kruk and M. Jaroniec, *J Am Chem Soc*, 2001, **123**, 1650-1657.
50. N. Suthiwangcharoen, T. Li, L. Wu, H. B. Reno, P. Thompson and Q. Wang, *Biomacromolecules*, 2014, **15**, 948-956.
51. T. Li, B. Ye, Z. Niu, P. Thompson, S. Seifert, B. Lee and Q. Wang, *Chem Mater*, 2009, **21**, 1046-1050.
52. W. Stöber, A. Fink and E. Bohn, *Journal of Colloid and Interface Science*, 1968, **26**, 62-69.
53. H.-s. Yun, S.-h. Kim, S. Lee and I.-h. Song, *Materials Letters*, 2010, **64**, 1850-1853.
54. F. Di Renzo, F. Testa, J. Chen, H. Cambon, A. Galarneau, D. Plee and F. Fajula, *Microporous and Mesoporous Materials*, 1999, **28**, 437-446.
55. T. A. Ostomel, Q. Shi, C. K. Tsung, H. Liang and G. D. Stucky, *Small*, 2006, **2**, 1261-1265.
56. B. Lei, X. F. Chen, Y. J. Wang, N. R. Zhao, C. Du and L. M. Fang, *J Biomed Mater Res A*, 2010, **94A**, 1091-1099.
57. C. Jiang, S. Hongli, W. Chengtie, D. Kerong and T. Tingting, *Biomaterials*, 2006, **27**.
58. C. Wu, Y. Zhou, C. Lin, J. Chang and Y. Xiao, *Acta Biomaterialia*, 2012.
59. Å. Rosengren, S. Oscarsson, M. Mazzocchi, A. Krajewski and A. Ravaglioli, *Biomaterials*, 2003, **24**, 147-155.
60. P. Ducheyne and Q. Qiu, *Biomaterials*, 1999, **20**, 2287-2303.
61. P. Valerio, M. M. Pereira, A. M. Goes and M. F. Leite, *Biomaterials*, 2004, **25**, 2941-2948.
62. I. D. Xynos, A. J. Edgar, L. D. K. Buttery, L. L. Hench and J. M. Polak, *Biochemical and Biophysical Research Communications*, 2000, **276**, 461-465.

Table 1 Specific surface area, Total pore volume and Pore size of MBGS

Samples	Specific surface area (m^2g^{-1})	Total pore volume (cm^3g^{-1})	Pore size (nm)
MBGS-1	115.132	0.685	2.302
MBGS-2	89.147	0.049	3.754
MBGS-3	40.191	0.023	4.354

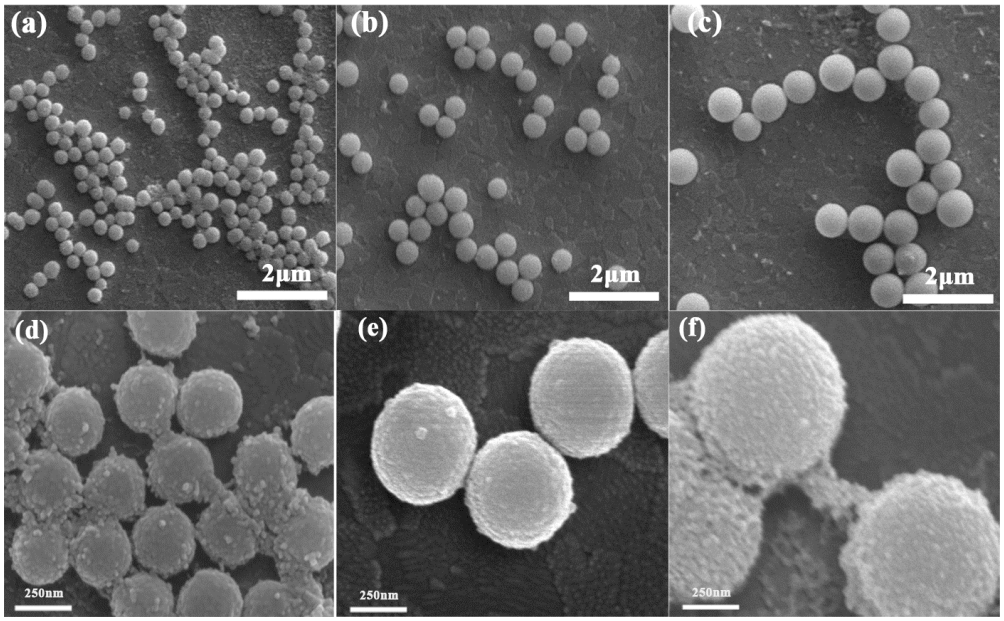

Fig. 1 SEM micrographs of MBGS obtained with different concentration of DDA at 0.08 mol/L (MBGS-1: a, d), 0.16 mol/L (MBGS-2: b, e) and 0.24 mol/L (MBGS-3: c, f).

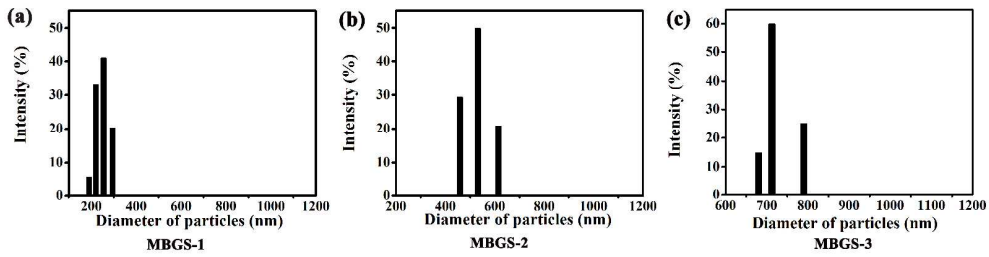

Fig. 2 Particle size distributions of MBGS-1 (a), MBGS-2 (b) and MBGS-3 (c).

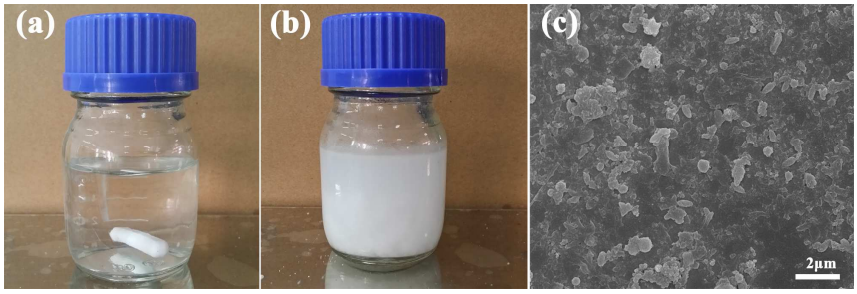

Fig. 3 The pictures for the state of the reaction solutions without the DDA (a), with the DDA (b) and SEM micrograph of BG obtained with the higher concentration of DDA at 0.4 mol/L (c)

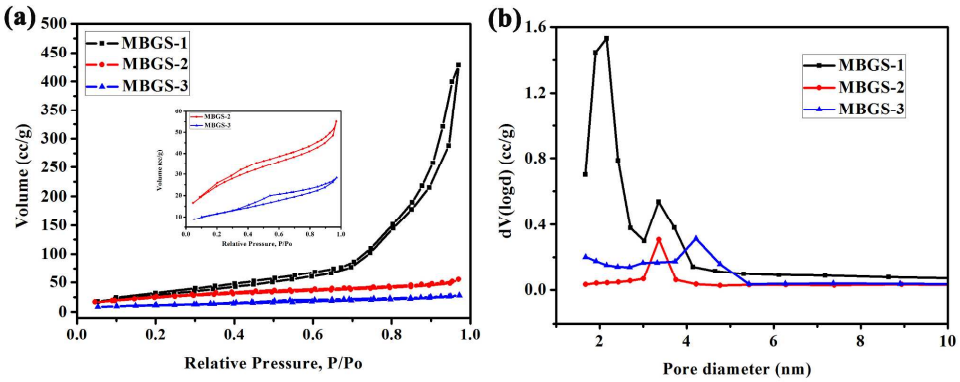

Fig. 4 N_2 absorption-desorption isotherm plots (a) and pore size distributions (b) of MBGS

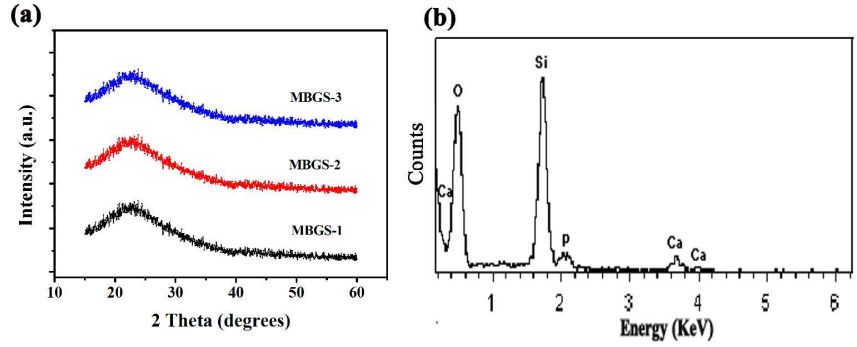

Fig. 5 Structure and compositions of MBGS. (a) XRD patterns showing the amorphous structure of MBGS; (b) EDS analysis showing the element composition of MBGS.

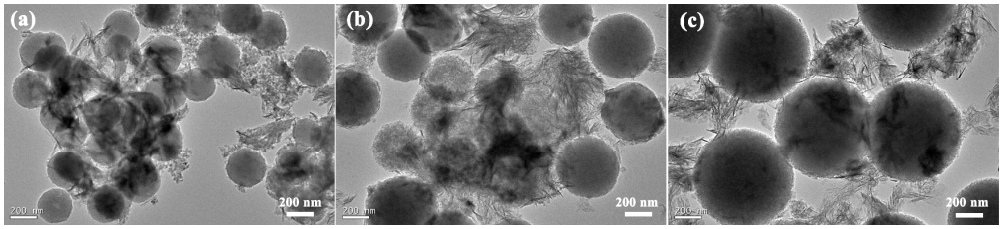

Fig. 6 TEM images of MBGS-1 (a), MBGS-2 (b) and MBGS-3 (c) after soaking in SBF for 3 days.

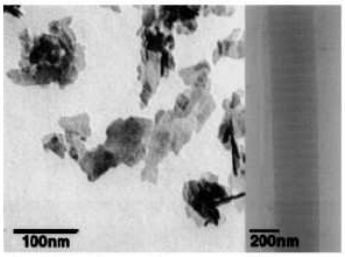

Fig. 7 TEM image of natural nanoscale apatite crystal [46]

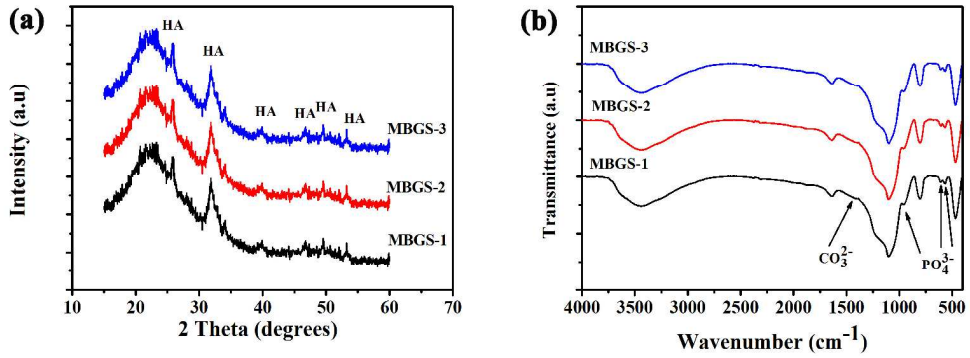

Fig. 8 XRD patterns (a) and FT-IR spectra (b) of all the MBGS after soaking in SBF for 3 days.

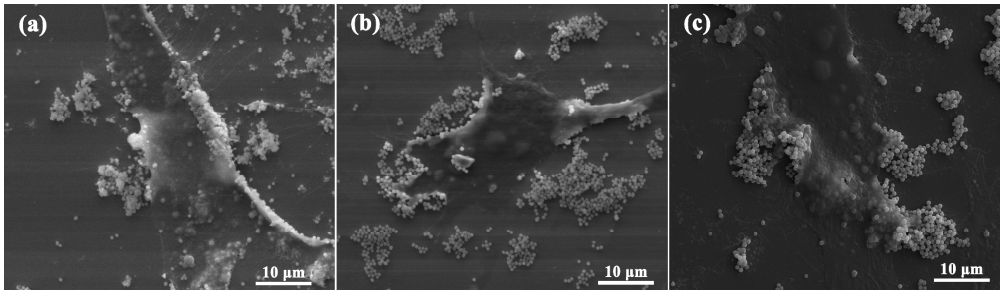

Fig. 9 Cells morphology after culturing on MBGS-1 (a), MBGS-2 (b) and MBGS-3 (c) for 4 hours.

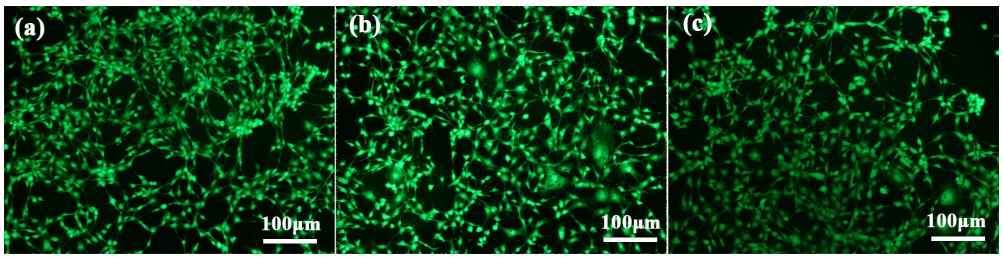

Fig. 10 FM images of cells cultured on MBGS-1 (a), MBGS-2 (b) and MBGS-3 (c) for 3 days.

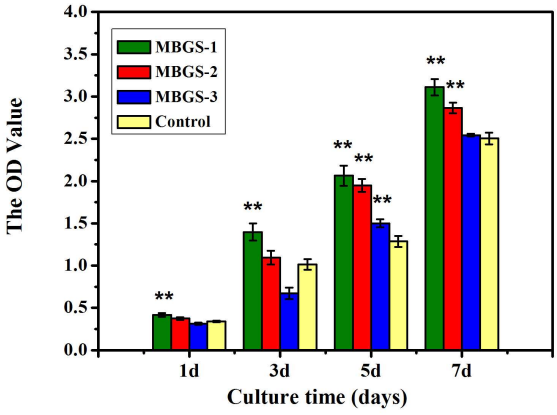

Fig. 11 Cells proliferation at different culture times on MBGS, date were represented as mean ± SD, n= 6; differences were considered significant when **P < 0.01, *P < 0.05. OD means optic density.

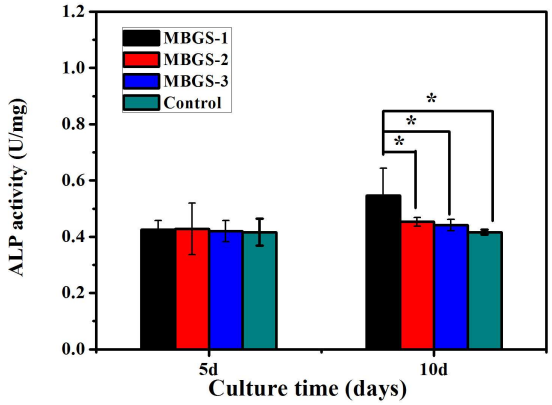

Fig. 12 ALP activity expression of cells after culturing on MBGS for 5 and 10 days, date was represented as mean ± SD, n = 3; differences were considered significant when *P < 0.05.

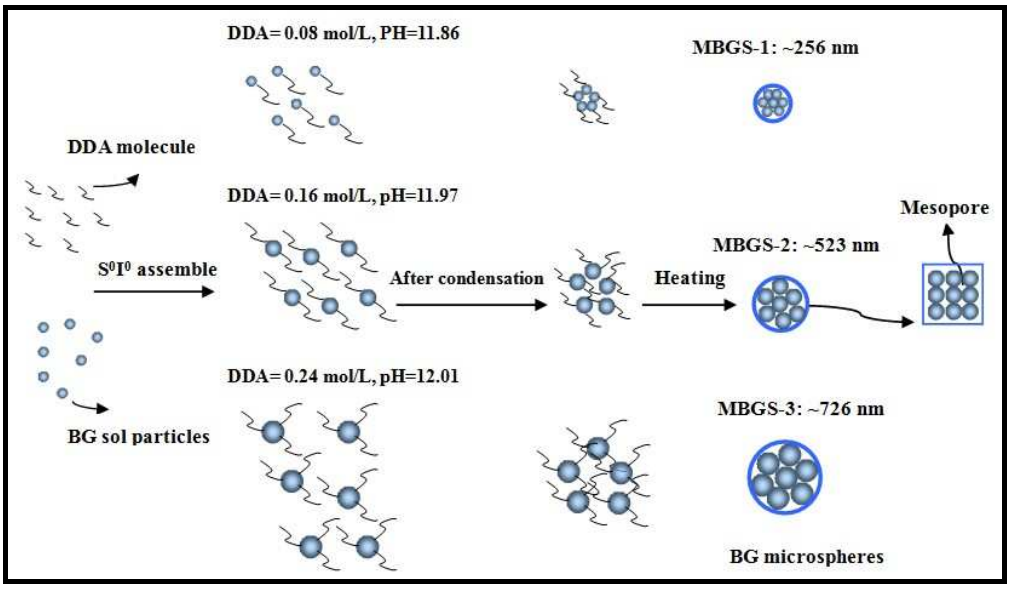

Fig. 13 Schematic illustration of the formation processes of MBGS with controllable particle size.